An Assessment of Satellite and Radiosonde Climatologies of Upper-Tropospheric Water Vapor

BRIAN J. SODEN AND JOHN R. LANZANTE

Geophysical Fluid Dynamics Laboratory, National Oceanic and Atmospheric Administration, Princeton, New Jersey

(Manuscript received 2 May 1995, in final form 15 September 1995)

ABSTRACT

This study compares radiosonde and satellite climatologies of upper-tropospheric water vapor for the period 1979–1991. Comparison of the two climatologies reveals significant differences in the regional distribution of upper-tropospheric relative humidity. These discrepancies exhibit a distinct geopolitical dependence that is demonstrated to result from international differences in radiosonde instrumentation. Specifically, radiosondes equipped with goldbeater's skin humidity sensors (found primarily in the former Soviet Union, China, and eastern Europe) report a systematically moister upper troposphere relative to the satellite observations, whereas radiosondes equipped with capacitive or carbon hygristor sensors (found at most other locations) report a systematically drier upper troposphere. The bias between humidity sensors is roughly 15%–20% in terms of the relative humidity, being slightly greater during summer than during winter and greater in the upper troposphere than in the midtroposphere. However, once the instrumentation bias is accounted for, regional variations of satellite and radiosonde upper-tropospheric relative humidity are shown to be in good agreement. Additionally, temporal variations in radiosonde upper-tropospheric humidity agree reasonably well with the satellite observations and exhibit much less dependence upon instrumentation.

The impact that the limited spatial coverage of the radiosonde network has upon the moisture climatology is also examined and found to introduce systematic errors of 10%–20% relative humidity over data-sparse regions of the Tropics. It is further suggested that the present radiosonde network lacks sufficient coverage in the eastern tropical Pacific to adequately capture ENSO-related variations in upper-tropospheric moisture. Finally, we investigate the impact of the clear-sky sampling restriction upon the satellite moisture climatology. Comparison of clear-sky and total-sky radiosonde observations suggests the clear-sky sampling limitation introduces a modest dry bias (<10% relative humidity) in the satellite climatology.

1. Introduction

Water vapor is widely recognized to be of fundamental importance in determining climate and its sensitivity to increasing greenhouse gases. While lower-tropospheric water vapor is generally accepted to provide a positive feedback within the climate system, there is less consensus regarding the role of upper-tropospheric water vapor. Much of the uncertainty surrounding upper-tropospheric water vapor stems from concerns regarding our ability to accurately measure its distribution and climatological variations. Potential problems in radiosonde observations are frequently cited (e.g., Elliott and Gaffen 1991). Consequently, an improved understanding of the climatic role of upper-tropospheric moisture requires an accurate assessment of our present ability to monitor it on a global scale. In this study, we compare two of the largest global moisture archives—radiosonde observations and satellite infrared measurements—to quantitatively evaluate our ability to observe climatological variations in upper-tropospheric water vapor.

Satellite observations of the upwelling infrared radiation in the 6.3-μm water vapor absorption band provide a unique source of information on tropospheric water vapor. The TIROS Operational Vertical Sounder (TOVS) carried on board the NOAA series of polar-orbiting satellites contains three water vapor channels located at 6.7, 7.3, and 8.3 μm that are sensitive to relative humidity in the upper, middle, and lower troposphere, respectively. Water vapor radiance measurements are available two to four times per day with near-global coverage from February 1979 to the present. This combination of high spatial–temporal coverage and long duration is unmatched by any other water vapor archive. The chief limitations of these measurements are their poor vertical resolution and their restriction to clear and partially cloudy conditions.

The radiosonde network has long been the primary observing system for monitoring tropospheric water

Corresponding author address: Dr. Brian J. Soden, Geophysical Fluid Dynamics Laboratory/NOAA, P.O. Box 308, Princeton, NJ 08542.
E-mail: bjs@gfdl.gov

vapor. Radiosonde observations have the advantage of providing high vertical resolution, measurements under clear and cloudy conditions, and a long historical record (dating back to the early 1950s). The radiosonde observations are limited by their restricted spatial coverage, reduced accuracy in the upper troposphere, and inhomogeneities resulting from changes in instrumentation and reporting practices.

This study investigates the climatological variations of upper-tropospheric water vapor determined from radiosonde and satellite observations. Section 2 describes the datasets and comparison procedures used in this study. Section 3 analyzes the regional and temporal variations of upper-tropospheric water vapor. Section 4 investigates the impact of the limited spatial coverage upon the radiosonde water vapor climatology, and section 5 examines the impact of the clear-sky sampling restriction upon the satellite water vapor climatology. A discussion of our conclusions is provided in section 6.

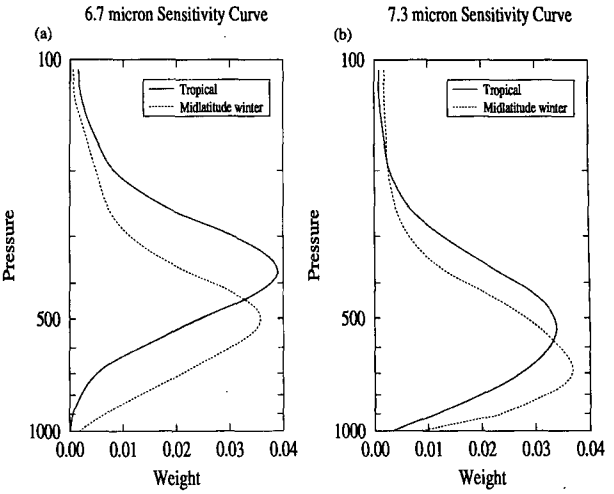

FIG. 1. Sensitivity of $T_{6.7}$ (a) and $T_{7.3}$ (b) to local perturbations of 10% relative humidity in thin layers, equally spaced in log pressure (dp/p = 0.04). Curves are shown separately for a typical tropical (solid) and a midlatitude winter (dashed) profile. The sum of the weights over pressure is equal to unity.

2. Data and analysis procedure

a. TOVS water vapor radiances

1) DATA CHARACTERISTICS

Several recent studies have employed satellite observations in the 6.3-μm water vapor absorption band to describe the distribution of water vapor in the upper troposphere (Schmetz and Turpeinen 1988; Soden and Bretherton 1993; Wu et al. 1993; Soden and Fu 1995). This paper makes use of 6.7-μm spectral measurements made by TOVS. The 6.7-μm channel is located near the center of a strong water vapor absorption band and is primarily sensitive to relative humidity in the upper troposphere (Soden and Bretherton 1993). Figure 1a shows the sensitivity of the 6.7-μm brightness temperature ($T_{6.7}$) to local variations in relative humidity for typical tropical and midlatitude winter profiles. Two points are illustrated in this figure. The first is that $T_{6.7}$ does not measure water vapor at a single level, rather it is sensitive to variations in moisture over a broad layer centered in the upper troposphere (roughly 200–500 mb). The second point is that this layer is not fixed but shifts vertically depending upon the nature of the atmosphere—it is slightly lower for cold–dry profiles (e.g., midlatitude winter) and slightly higher for warm–moist profiles (e.g., tropical).

Since clouds strongly attenuate the infrared radiation, estimation of the upper-tropospheric humidity requires information from pixels in which the radiance emitted to space is not affected by cloud cover. In this study we use the clear and cloud-cleared (up to 75% cloud cover) radiances produced by the National Environmental Satellite Data and Information Service (NESDIS) using the "N*" technique (McMillin and Dean 1982). These data are archived in the operational sounding product data set (Kidwell 1991). A thorough description and error analysis of this dataset is provided by Wu et al. (1993). Since the spectral response function of the 6.7-μm channel differs slightly between individual satellites, the TOVS data are gridded separately for each satellite (*TIROS-N, NOAA-6* to *NOAA-11*) onto daily 2.5° latitude by 2.5° longitude grids for the period February 1979–December 1991.

As mentioned earlier, one limitation of the TOVS water vapor radiances is their restriction to clear and partially cloudy conditions. Since cloudiness is correlated with relative humidity, the lack of measurements from areas of extensive cloud cover is likely to introduce a dry bias into the satellite climatology. Unfortunately, the magnitude of the bias is largely unknown. In section 5 of this study, we attempt to quantify this bias by comparing the total-sky radiosonde climatology with a clear-sky radiosonde climatology containing the identical sampling restrictions present in the satellite data.

2) UPPER-TROPOSPHERIC HUMIDITY

Although 6.7-μm brightness temperatures are a valuable source of information on upper-tropospheric water vapor, for interpretation purposes it is useful to relate the brightness temperatures to a more familiar water vapor quantity. Soden and Bretherton (1993) addressed this issue by developing a simplified treatment of radiative transfer based upon a random strong line model, which provides a convenient means of interpreting 6.7-μm brightness temperatures in terms of a vertically averaged upper-tropospheric relative humidity (UTH). The UTH corresponds to the relative humidity weighted according to the 6.7-μm sensitivity curve for that particular sounding and thus represents

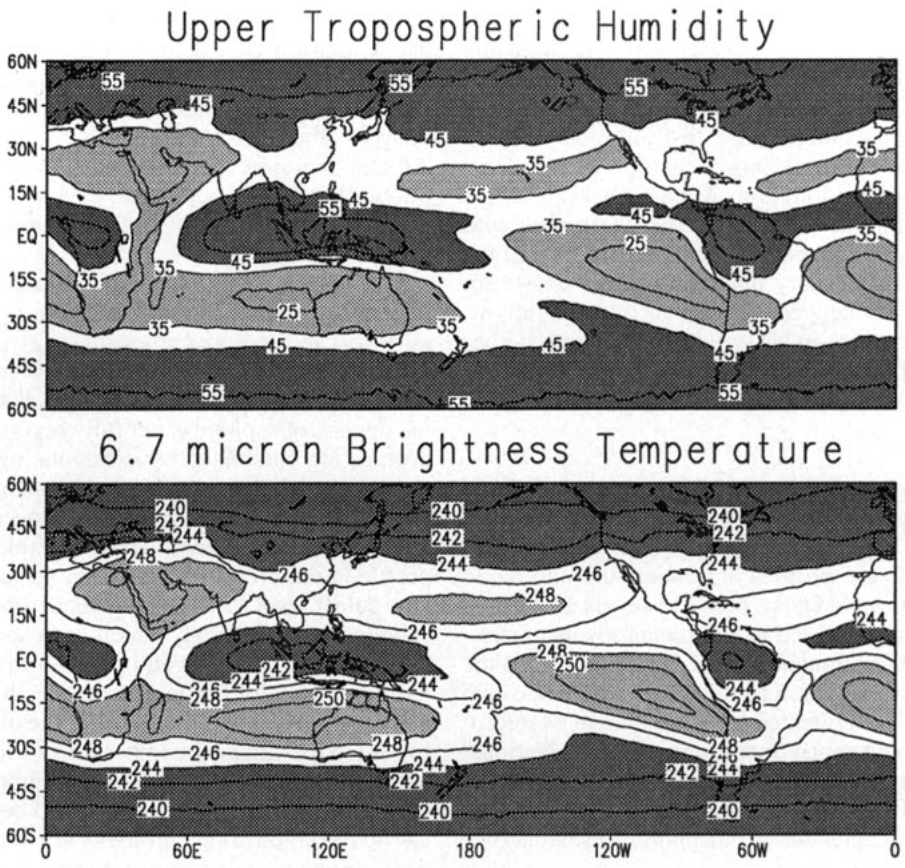

FIG. 2. Map of annual average upper-tropospheric relative humidity (top) in percent and $T_{6.7}$ (bottom) in K from the TOVS for the period 1979–1991.

a vertically averaged value over a layer extending from roughly 200 to 500 mb (e.g., Fig. 1). Using the Goody random band model (Goody 1964) and assuming strongly absorbing, pressure-broadened lines, Soden and Bretherton (1993, 1995) demonstrated that the 6.7-μm brightness temperature ($T_{6.7}$) varies logarithmically with the UTH according to

$$\ln\left(\frac{\text{UTH}\, p_0}{\cos\theta}\right) = a + bT_{6.7}, \qquad (1)$$

where θ is the satellite-viewing zenith angle, $a = 31.50$, $b = -0.1136\ \text{K}^{-1}$ are regression coefficients, and p_0 is a normalized reference pressure of the 240 K isotherm. The coefficients a, b are determined by comparing synthetic $T_{6.7}$, calculated from representative profiles of temperature and moisture, with the corresponding vertically averaged upper-tropospheric relative humidity obtained from the same profiles. These coefficients are in good agreement with the theoretically expected values and are not sensitive to the particular profile dataset used to derive them (Soden et al. 1994; Soden and Bretherton 1996). In processing the satellite observations, NESDIS converts radiances viewed at a variety of viewing angles to equivalent nadir-view ($\theta = 0$) radiances, therefore $\cos\theta = 1$ in Eq. (1). The reader is referred to Soden and Bretherton (1993, 1996) for details of the random strong line model and derivation of Eq. (1).

The TOVS instrument also contains a second water vapor channel centered at 7.3 μm. This channel is located farther from the center of the 6.3-μm water vapor band and consequently measures relative humidity over a slightly deeper layer of atmosphere (e.g., Fig. 1b). As demonstrated by Soden and Bretherton (1996), the 7.3-μm brightness temperatures may also be interpreted in terms of a middle tropospheric relative humidity (MTH) using a relationship analogous to Eq. (1) with $a = 29.89$ and $b = -0.0996\ \text{K}^{-1}$. Here the MTH corresponds to the relative humidity averaged over a broad layer centered in the midtroposphere (roughly 400–800 mb). Observations of midtropospheric relative humidity are used in section 3 to examine the vertical dependence of discrepancies between the satellite and radiosonde climatologies.

An illustration of the moisture climatology obtained from the 6.7-μm channel is presented in Fig. 2. This diagram shows a map of the annual mean $T_{6.7}$ for the

period 1979–1991 and the corresponding UTH determined from Eq. (1). Since water vapor reduces the infrared emission to space, warm $T_{6.7}$ correspond to a dry upper troposphere and cold $T_{6.7}$ correspond to a moist upper troposphere. The distributions of both UTH and $T_{6.7}$ reflect well-known features of the large-scale atmospheric circulation. Maximum UTH occur along the equator and western Pacific warm pool with minima over the subtropical descending branches of the Hadley cell and secondary maxima over the extratropics. The similarity between these two maps highlights the fact that variations in UTH closely reflect variations in the $T_{6.7}$ field.

b. *Radiosonde data*

This study uses archives of 12-hourly (0000 and 1200 UTC) observations from the global network of approximately 850 radiosonde stations for the period 1979–1991. We use profiles of temperature and moisture reported on mandatory pressure levels as well as any observations provided at significant levels to compute a radiosonde-simulated UTH (as described in the next section) for each 12-h profile. The radiosonde data examined here are collected by the National Meteorological Center (currently incorporated in the National Centers for Environmental Prediction) via the global telecommunications network and archived by R. Jenne at the National Center for Atmospheric Research.

c. *Comparison procedure*

One difficulty in comparing the satellite and radiosonde datasets is that they measure fundamentally different quantities. The satellites measure radiances, while the radiosondes provide vertical profiles of temperature and moisture. Therefore, to compare the satellite and radiosonde measurements, a two-step "profile to satellite" procedure is used. In the first step, radiosonde profiles of temperature and moisture are inserted into the operational TOVS transmittance model (Weinreb et al. 1981) to simulate a $T_{6.7}$, which would be observed by the satellite from a nadir viewing geometry under those conditions. The second step transforms both the satellite-observed $T_{6.7}$ and the radiosonde-simulated $T_{6.7}$ into UTH quantities using Eq. (1). In this way, the observed and simulated $T_{6.7}$ are treated in a consistent manner. Therefore, the transformation from radiance to humidity does not cause spurious differences between the satellite and radiosonde UTH because the same transformation is applied to both. Essentially, it is $T_{6.7}$ that is compared, only the comparison is performed in UTH space rather than brightness temperature space to facilitate interpretation of the results in terms of a more familiar water vapor quantity. Generally speaking, the forward calculations (profile to radiance) are by definition more accurate than inverse calculations (radiance to geophysical quantity) since, at some level, the inverse calculations use a forward model to do the retrieval. Hence, this approach provides the accuracy of comparing observed radiances with simulated radiances as well as an easily interpretable measure of upper-tropospheric moisture. An identical procedure was used by Soden and Bretherton (1994) and Soden et al. (1994) to compare GCM and Raman lidar profiles of moisture with GOES observations of $T_{6.7}$.

One of the limitations with the radiosonde dataset is that, for certain locations, moisture is not reported at all levels in the upper troposphere, while accurate radiative transfer calculations require moisture profiles up to 100 mb. In situations where relative humidity in the upper troposphere is not fully reported, the moisture profiles are completed by extrapolating from the highest reported level up to 100 mb assuming a constant relative humidity. To restrict the uncertainty resulting from this extrapolation, the actual radiosonde moisture profile is required to be reported up to at least −40°C [the cutoff level for U.S. radiosondes during this period (Garand et al. 1992)], which corresponds to roughly 250 mb in the Tropics and 350 mb in the winter midlatitudes. Relative humidity above these levels typically contributes less than 15% to the observed $T_{6.7}$ (see Fig. 1). To estimate the impact of this filling procedure, we compared 6.7-μm brightness temperatures calculated from a sample of over 12 000 complete (i.e., up to 100 mb) radiosonde profiles with the brightness temperature calculated using the same set of profiles but assuming a constant relative humidity above 300 mb (e.g., for each sounding the relative humidity above 300 mb was set replaced with the 300-mb relative humidity from that particular sounding). The profiles used here were instantaneous soundings collected from an array of over 200 geographically dispersed stations. The comparison suggests that the use of a constant relative humidity assumption to fill incomplete profiles has only a small impact upon the simulated monthly mean $T_{6.7}$ for each station, introducing an additional rms uncertainty of ~0.7 K (or ~4% relative humidity in terms of UTH) with a bias of ~0.5 K (roughly −3% relative humidity). These uncertainties are about a factor of 5 or more smaller than the typical regional or seasonal variations in UTH examined here (see Figs. 4 and 9). The relatively small impact of the filling procedure is consistent with climatological water vapor profiles determined from SAGE II (McCormick and Chiou 1994, see their Figs. 3 and 4 and Table 2), which suggest that the seasonal-mean vertical profile of relative humidity in the uppermost part of the troposphere is in fact very nearly constant. For example, typical SAGE relative humidity lapse rates ($d\mathrm{rh}/dz$) between 300 and 200 mb vary from roughly +2% km^{-1} to −3% km^{-1}.

Another source of uncertainty in the comparison can arise from errors in the radiative transfer calculations. An error analysis of the operational TOVS transmit-

tance model (OTTM) by Murty et al. (1993) suggested systematic discrepancies of 1–2 K in the $T_{6.7}$ as compared to line by line calculations. Similar results were found when we compared radiances from the OTTM with those calculated from the RTTOVS transmittance model (Eyre 1991) using profiles from the TIGR dataset. The TIGR profile dataset is collection of roughly 1700 soundings carefully selected to be representative of the global atmosphere at any time and place (Monine et al. 1987). Statistics from the comparison are listed in Table 1. Radiances from the OTTM model were found to be highly correlated with the RTTOVS calculations (r = 0.99) but systematically warmer by ~1.8 K. The high correlation indicates that there is little regional dependence to the differences; however, the consistency of the bias with that of Murty et al. (1993) suggests that the OTTM calculations may be systematically too warm by 1–2 K. To minimize the impact that uncertainties in the forward calculations have upon our results, the subsequent analysis will focus on using the satellite observations as a fixed reference, rather than an absolute reference, for comparing the radiosonde-simulated radiances. Further discussion of the impact of this uncertainty upon the analysis is provided section 3a.

For each available 12-hourly radiosonde profile that extends up to the required height (i.e., the −40°C isotherm), the temperature and moisture profiles are inserted into the operational TOVS transmittance model (using the appropriate spectral response function for the satellite in orbit at that time) to yield a simulated $T_{6.7}$ that would be observed by the satellite under those conditions. If more than one satellite was operational, then separate simulations were performed using the appropriate spectral response functions for each satellite. For each 12-hourly sounding, the radiosonde-simulated $T_{6.7}$ values are then transformed into UTH values using Eq. (1). All available 12-hourly UTH are then composited into monthly averages for the period February 1979–December 1991. Likewise, for each orbital pass the satellite clear-sky $T_{6.7}$ (when available) is converted into UTH using the identical transformation and composited into monthly averages for the same period. No attempt is made to ensure that the both the radiosonde and satellite monthly averages contain observations from the same subset of days within the month so as not to introduce a clear-sky sampling bias into the radiosonde climatology (see section 5). We do note, however, that imposing such a constraint does not affect any of the conclusions reported here.

3. Comparison of upper-tropospheric humidity climatologies

a. Regional variations

In this section we compare the regional distributions of upper-tropospheric moisture from the satellite and radiosonde observations. Figure 3a shows a map of the difference between the radiosonde and satellite upper-tropospheric relative humidity averaged over the 3-month period June, July, and August 1989. At each radiosonde location, the difference in UTH (radiosonde−satellite) is plotted numerically (expressed as a percentage relative humidity) and color coded according to the scale at the bottom. Roughly 25% of the 850 or so archived radiosonde stations are not shown in Fig. 3 because they did not contain a sufficient number of upper-level moisture profiles to permit calculation of the $T_{6.7}$ (a minimum of 20 profiles per month were required). The missing stations are scattered primarily across Europe, Asia, Africa, and South America with a local cluster of missing stations in India.

TABLE 1. The bias (OTTM − RTTOVS), rms difference, and correlation between forward calculated $T_{6.7}$ from the operational TOVS transmittance model (OTTM) and from the RTTOVS model. Calculations were made using the TIGR profile dataset.

Bias	Rms	Correlation
1.8 K	2.0 K	0.99

The chief feature of Fig. 3 is the distinct geopolitical dependence of the differences between radiosonde and satellite UTH. Over most of the former Soviet Union, China, and eastern Europe, the vast majority of radiosondes indicate a systematically moister upper troposphere relative to the satellite (*NOAA-10*), whereas over the rest of the globe (e.g., North America, western Europe, Africa, Australia, Indonesia) the radiosondes generally indicate a systematically drier upper troposphere relative to the satellite. These differences often exceed 10%–15% relative humidity or roughly 3–4 K in terms of $T_{6.7}$. Since the same satellite is used in the comparison at all radiosonde locations, the satellite measurements serve as a fixed but not absolute reference. Thus, we can infer that radiosondes values over the former Soviet Union tend to be systematically moister than the satellite measurements that are, in turn, systematically moister than radiosonde values over western Europe. However, it is not obvious from these data which of the three sets of measurements is correct in an absolute sense. That is, all three measurements could be in error relative to the actual atmosphere. Radiosondes have widely recognized difficulties in measuring upper-tropospheric moisture (Elliott and Gaffen 1990). The satellite measurements may suffer from uncertainties in calibration (e.g., Bates and Wu 1996). However, such a satellite calibration error would introduce a systematic bias at all locations and would not be regionally dependent like the bias shown in Fig. 3. Similarly, the errors in the radiance calculations may introduce a systematic bias in the radiosonde-simulated $T_{6.7}$. However, these errors are also systematic rather than regionally dependent (see Table 1).

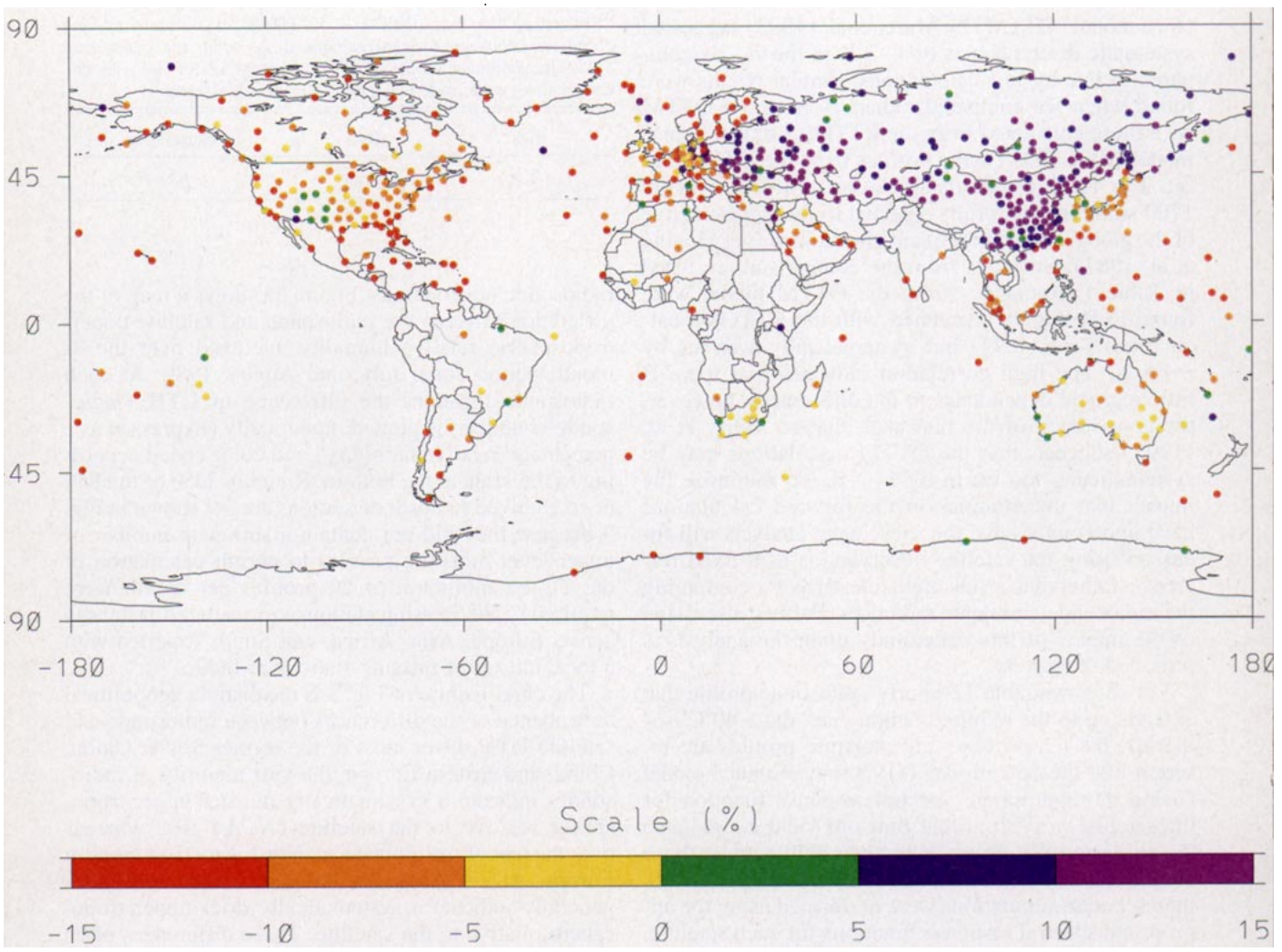

FIG. 3. Map of the difference in upper-tropospheric relative humidity (radiosonde–satellite) for JJA 1989.

The accuracy of the radiosonde measurements depends largely upon the type of humidity sensor used, which frequently differs from one country to the next. This difference in radiosonde instrumentation is thus the leading candidate to explain the strong regional dependence of the UTH differences. To investigate this hypothesis, each radiosonde location was categorized into two groups based upon the humidity sensor in use as determined from station history documentation (Gaffen 1993; Oakley 1993). Type-A radiosondes consist of those using goldbeater's skin humidity sensors (e.g., MARS, MRZ, A-22, GZZ, Mark 3). The goldbeater's skin is an electromechanical sensor composed primarily of animal tissue that shrinks or expands as the relative humidity changes, resulting in mechanical movements that are registered using an Olland cycle (Middleton and Spilhaus 1953). Type-B radiosondes primarily consist of carbon hygristor or capacitive (e.g., Humicap) humidity sensors (e.g., VIZ, Vaisala, AIR, SDD, Meisei, Phillips). These are electrical sensors in which the resistance or capacitance varies as a function of relative humidity. Figure 4 compares the satellite and radiosonde UTH for JJA 1989. Each data point corresponds to an individual radiosonde station from Fig. 3, categorized into one of the two radiosonde groups. For all radiosonde stations, the correlation between the satellite and radiosonde UTH is 0.66, with an rms difference of 11.22% and bias (radiosonde–satellite) of 0.45%. The chief feature of this plot is the clear distinction between the individual radiosonde types. Type-A radiosondes equipped with goldbeater's skin sensors (which are primarily used in the former Soviet Union, China, and eastern Europe) systematically overestimate the UTH relative to the satellite observations, whereas type-B carbon hygristor and capacitive sensors (which are used at most other locations) systematically underestimate the UTH relative to the satellite. The type-B sensors in Fig. 4 are

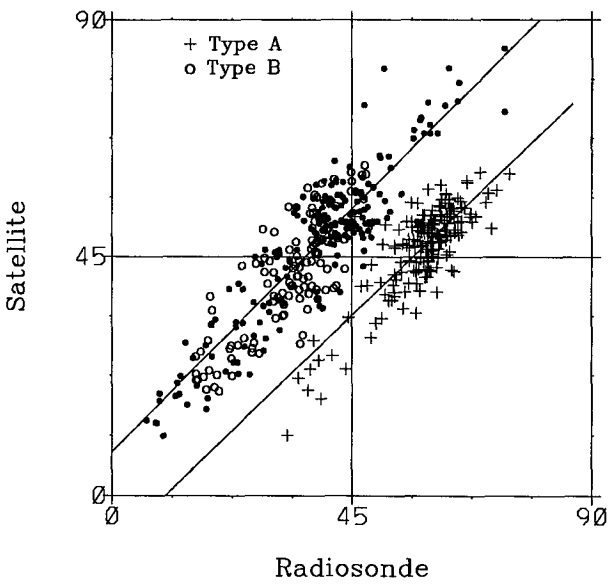

FIG. 4. Scatterplot of the radiosonde versus satellite UTH in percent categorized by sensor type for JJA 1989. Crosses indicate goldbeater's skin sensors (type A). Filled circles denote capacitive humidity sensors and open circles denote carbon hygristor sensors (type B). The lines represent least-squares fits calculated separately for type A and type B sensors.

further subdivided into capacitive (filled circle) and carbon hygristor (open circle) humidity sensors to search for systematic differences between these instruments. No clear distinction is apparent, indicating a relative degree of consistency between the UTH measurements from these two sensors.

An interesting feature in Fig. 3 occurs over the southwest United States where a cluster of radiosonde-satellite biases are systematically 8%–10% higher (and of the opposite sign) relative to the surrounding biases. This anomalous cluster corresponds to stations that used SDD radiosondes equipped with VIS-type carbon hygristor sensor. Since this sensor is identical to that used at all other U.S. stations, this feature cannot simply be attributed to instrumentation differences. Rather, the anomalous values reflect a documented error in the humidity conversion algorithm for SDD radiosondes that introduces a moist bias in the upper troposphere of ~5%–20% relative humidity (Wade 1995). This indicates that changes (or errors) in data reduction can also create spurious differences in the moisture climatology and suggests that comparisons with the satellite climatology are capable of detecting such changes.

Table 2 lists statistics of the comparison calculated for all radiosonde data and for types A and B individually. It is important to note that although the overall correlation between the satellite and radiosonde UTH is rather modest ($r \sim 0.66$), the correlation increases significantly when either type-A or -B radiosondes are considered individually ($r > 0.80$). If the bias between the satellite and radiosonde UTH is removed, then the rms difference reduces from 12.2% to 6.3% for type-A radiosondes and from 10.5% to 5.8% for type-B radiosondes in the case of JJA 1989. Thus, radiosonde and satellite observations of the regional variation in upper-tropospheric moisture are in good agreement provided that systematic differences in radiosonde instrumentation are accounted for. Furthermore, the distribution of points indicates that there is a near-constant bias between the two radiosonde types. This suggests that a first-order correction can be calculated empirically from Fig. 4 by performing a least-squares regression to each group individually (shown as solid lines in Fig. 4). Doing so leads to the following relation:

$$\mathrm{UTH_B} = 1.01\ \mathrm{UTH_A} - 18.05, \qquad (2)$$

where $\mathrm{UTH_A}$ ($\mathrm{UTH_B}$) is the seasonal-mean upper-tropospheric relative humidity for type-A (-B) radiosondes for JJA 1989. This indicates that, to a close approximation, the UTH reported by type-A radiosondes is uniformly higher by ~18% relative humidity compared to type-B radiosondes. Applying this adjustment to the JJA 1989 data increases the correlation between satellite and radiosonde UTH from 0.66 to 0.86 and reduces the rms difference from 11.2% to 6.1%.

The bias between type-A and -B radiosondes is a robust feature of the comparison that persists throughout the duration of available satellite data. Figure 5 shows scatterplots of satellite versus radiosonde UTH for JJA of 1979, 1982, 1985, and 1991. Each period

TABLE 2. The correlation, rms difference, and bias between radiosonde and satellite observations of upper-tropospheric humidity. Statistics are calculated separately for all radiosondes, type-A radiosondes, and type-B radiosondes. Results for six different periods are shown with the satellite used for each period listed in parentheses.

		Correlation	Rms difference	Bias (raob − sat)
JJA 1989	All	0.66	11.2%	−0.5%
(*NOAA-10*)	Type A	0.83	12.2%	11.2%
	Type B	0.88	10.7%	−8.5%
JJA 1979	All	0.67	11.2%	10.1%
(*TIROS-N*)	Type A	0.76	19.2%	18.3%
	Type B	0.85	9.6%	−1.1%
JJA 1982	All	0.62	12.1%	1.8%
(*NOAA-6*)	Type A	0.77	12.2%	10.9%
	Type B	0.82	12.1%	−9.3%
JJA 1985	All	0.64	13.2%	4.5%
(*NOAA-7*)	Type A	0.82	17.4%	16.2%
	Type B	0.85	8.1%	−4.5%
JJA 1991	All	0.64	12.1%	−3.0%
(*NOAA-11*)	Type A	0.83	11.8%	10.0%
	Type B	0.87	12.1%	−10.1%
DJF 1989	All	0.70	10.7%	−2.3%
(*NOAA-10*)	Type A	0.77	10.6%	6.3%
	Type B	0.82	10.3%	−7.2%

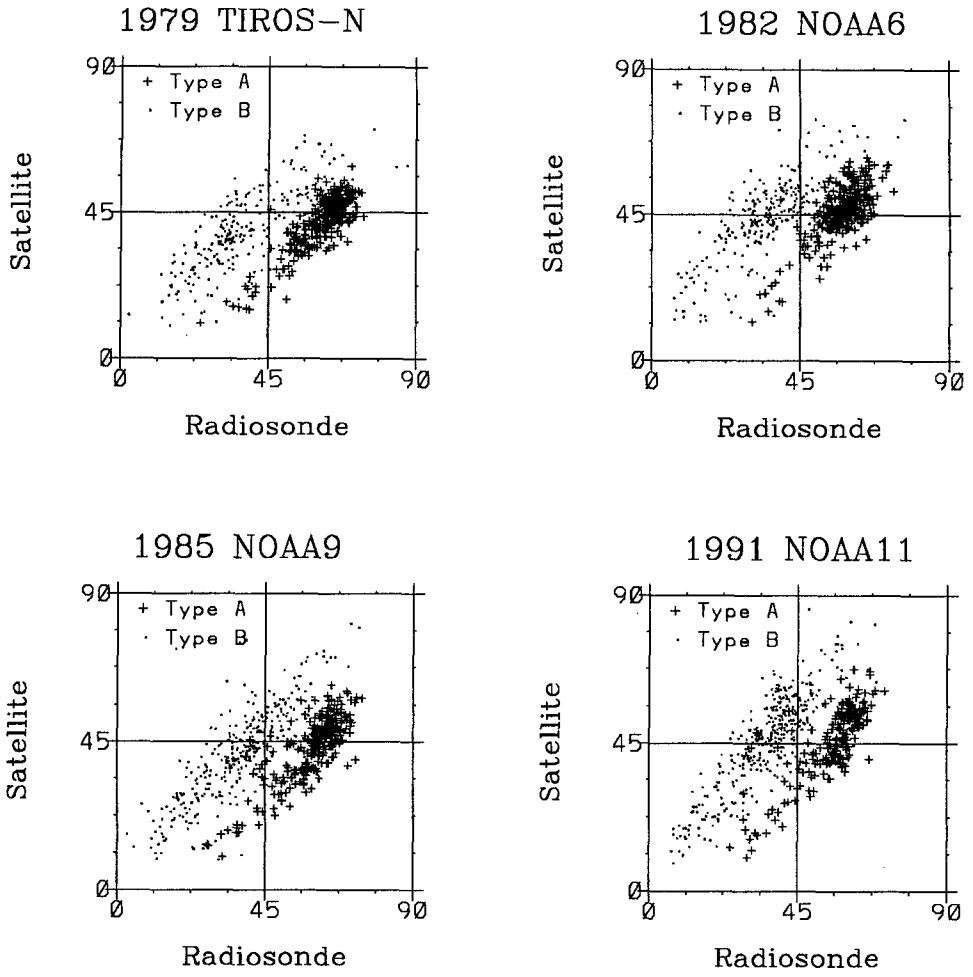

FIG. 5. Scatterplot of radiosonde versus satellite UTH in percent for JJA 1979 (a), 1982 (b), 1985 (c), and 1991 (d).

corresponds to a different operational satellite, *TIROS-N, NOAA-6, NOAA-9,* and *NOAA-11,* respectively. Statistics of the comparison are listed in Table 2 for each period. During all four periods, measurements from type-A radiosondes are systematically moister than the satellite observations, while measurements from type-B radiosondes are systematically drier than the satellite observations. Also note that the bias between a particular radiosonde type and the satellite observations varies slightly from one satellite to the next, possibly reflecting differences in calibration of the TOVS instrument (e.g., Bates and Wu 1996). However, the difference between type-A and type-B measurements remains at a nearly constant value of 18%–20%, in good agreement with the adjustment proposed in Eq. (2). A slightly greater dispersion is apparent within the type-B distribution for 1979, which may reflect inaccurate classification of the humidity sensor due to limitations in the radiosonde history documentation for earlier time periods. The type-B radiosondes also exhibit a greater range of UTH than the type-A radiosondes, reflecting the differing spatial distribution of the instruments. The type-A radiosondes are primarily restricted to the extratropics, whereas the type-B radiosondes are found over a much wider range of latitudes, including the Tropics and subtropics where regional variations in UTH are largest (see Fig. 2).

Figure 6 compares the satellite versus radiosonde UTH for the period December 1988–February 1989 (DJF 1989). The dependence upon radiosonde instrumentation is qualitatively similar to that noted for JJA, indicating that it is not restricted to a particular season. However, the magnitude of the bias between type-A and type-B radiosondes is slightly smaller during DJF compared to JJA. This feature, which is also present for other DJFs, results from both type-A and type-B radiosonde measurements moving closer toward the satellite measurements (i.e., type-A measurements have less of a dry bias relative to the satellite and type-B measurements less of a moist bias). Hence, the over-

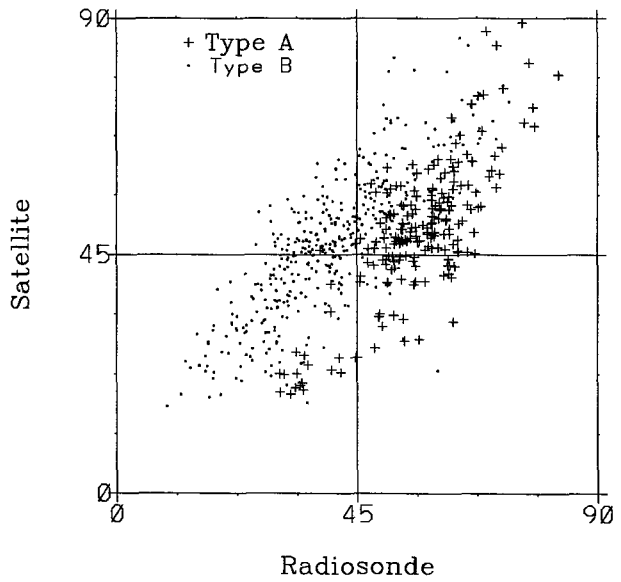

FIG. 6. Scatterplot of the radiosonde versus satellite UTH in percent for DJF 1989.

all agreement between the satellite and radiosonde observations tends to be slightly better during DJF than JJA (see Table 2). The reason for this apparent seasonal dependence is presently unknown. One possible explanation may be that since DJF is the winter season for the vast majority of the radiosonde locations, the layer to which the $T_{6.7}$ is sensitive will, on average, be slightly lower during DJF than during JJA. Since radiosondes are generally considered to be more reliable (and hence more consistent) at lower levels, this may explain the reduced discrepancy observed during DJF.

The observation that measurements from type-A sensors are systematically moister relative to type-B sensors is consistent with a longer response time for the older goldbeater's skin sensors relative to the newer carbon hygristor and capacitive sensors (Nash and Schmidlin 1987). The greater response time means that at any given height, the sensor is still responding to moisture at slightly lower levels in the atmosphere. Since the water vapor concentration decreases roughly exponentially with height, this leads to a systematic moist bias in the radiosonde profile. The response lag increases with decreasing temperature and thus its effects are most pronounced in the upper troposphere (Garand et al. 1992; Gaffen 1993). If response lags are responsible for the discrepancy between the two radiosonde types, then measurements at lower levels, where the response lag is smaller, would be expected to show better agreement. Figure 7 compares observations of the midtropospheric humidity (MTH) for JJA 1989 determined from satellite-observed and radiosonde-simulated 7.3-μm brightness temperatures ($T_{7.3}$). Compared to UTH, the MTH data exhibits better agreement between satellite and radiosonde observations, and the bias between type-A and -B radiosonde measurements is reduced roughly in half. This evidence reinforces the earlier conclusion that differences in sensor response time are largely responsible for the observed geopolitical bias in the radiosonde climatology.

It should also be mentioned that the dry bias of the type-B radiosonde relative to the satellite observations is qualitatively consistent with a possible warm bias in the radiative transfer calculations (see section 2c). This suggests that the type-B radiosondes (which are generally considered to be more accurate than their older type-A counterparts) and the satellite observations might be in better absolute agreement than indicated in Figs. 4–6, whereas the difference between type-A radiosondes and the satellite observations would become even greater. However, the systematic differences between the radiosonde and satellite measurements (roughly 3–4 K when expressed in terms of $T_{6.7}$) are roughly twice the estimated bias in the radiative transfer calculations (see section 2c). Thus, a systematic bias in the radiative transfer calculations are unlikely to explain all of the difference between the type-B radiosonde and satellite observations.

It is supposable that the differences between the satellite and radiosonde UTH noted in Fig. 3 could result from regional differences in atmospheric structure that might induce biases in either the satellite or radiosonde observations; however, this seems very unlikely given the strong correlation with instrumentation differences demonstrated in Figs. 4–6. Furthermore, the regional patterns exhibit sharp discontinuities in UTH along political boundaries (e.g., China, eastern Europe, and the former Soviet Union) that have no analog in atmospheric properties such as temperature or moisture (which could influence the accuracy of the radiosonde hygristors) or in cloud cover (which could influence

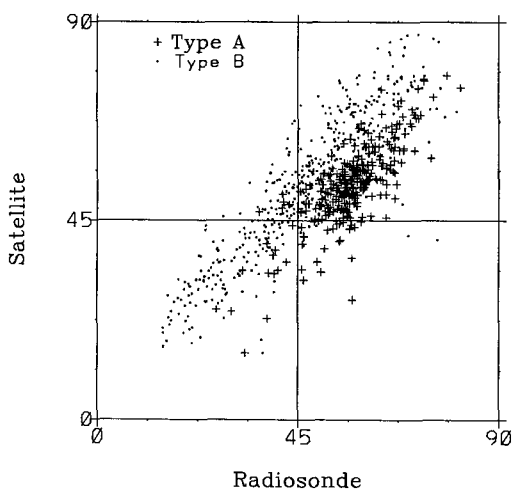

FIG. 7. Scatterplot of the radiosonde versus satellite MTH in percent for JJA 1989.

the satellite sampling). A unique illustration of the consistency between discontinuities in radiosonde UTH and geopolitical borders is given in Fig. 8. This figure depicts the radiosonde–satellite UTH for stations within the former German Democratic Republic. Four of the stations were operated by the GDR (WMO number beginning with "09") and used a MARS radiosonde equipped with a goldbeater's skin hygristor. The fifth station (10386) was located in West Berlin and operated by the former Free Republic of Germany, which used a Vaisala RS80 radiosonde equipped with a Humicap sensor. The goldbeater's skin sensor reported a systematically moister upper-troposphere relative to the satellite measurements, whereas the adjacent Humicap sensor is systematically drier relative to the satellite measurements. This is consistent with the above results and, given the close proximity of the stations, is clearly not related to regional differences in atmospheric structure.

b. Temporal variations

In this section we compare satellite and radiosonde observations of the temporal variation in upper-tropospheric water vapor. Figure 9 shows a scatterplot comparing the seasonal change in UTH (JJA 1989 minus DJF 1989) from satellite and radiosonde observations. Each data point corresponds to an individual radiosonde station and is categorized (as in Fig. 5) according to the type of humidity sensor used at that station. Overall there is good agreement between the radiosonde and satellite seasonal differences in upper-tropospheric moisture. Both datasets exhibit a similar range of seasonal variability and the correlation between the satellite and radiosonde observations is 0.84, with an rms difference of 8.1%. Since the instrumentation-dependent bias between the satellite and radiosonde measurements is roughly similar for both the summer and winter seasons, calculating the seasonal difference removes much of this difference. Consequently, the satellite and radiosonde seasonal changes exhibit only a small dependence upon radiosonde type.

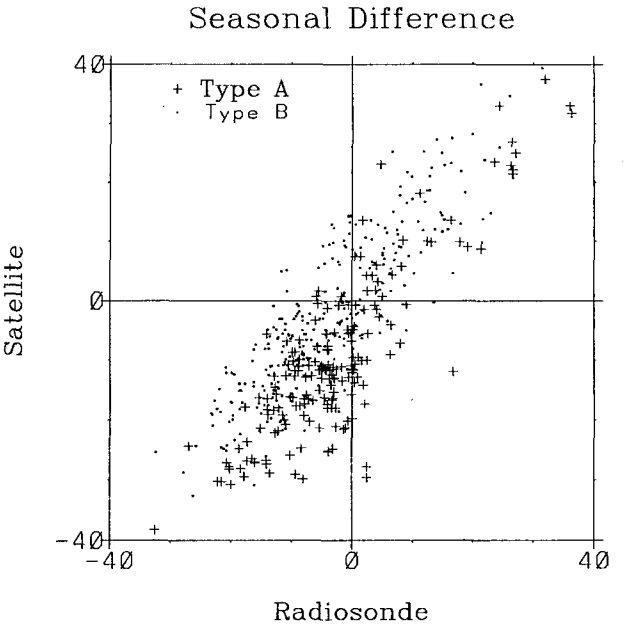

FIG. 9. Scatterplot of the radiosonde versus satellite seasonal difference (JJA minus DJF) of UTH in percent for 1989.

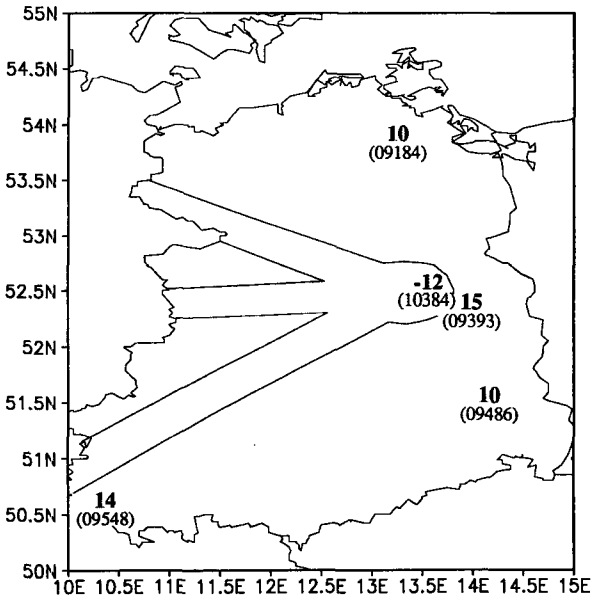

FIG. 8. The difference in UTH (satellite − radiosonde) in percent over the former German Democratic Republic (East Germany) for JJA 1989. WMO numbers (shown in parentheses) starting with "09" indicate East German stations that used goldbeater's skin sensors. WMO 10384 is a West German station located in West Berlin that used a Humicap sensor.

Further illustration of the temporal behavior of the radiosonde and satellite upper-tropospheric humidity measurements is presented in Fig. 10. This plot compares a time series of monthly mean radiosonde and satellite UTH from three different radiosonde stations for the period October 1979–June 1991. Each of the three radiosonde stations used a different type of humidity sensor. Specifically, Caroline Islands (WMO 91413) used a VIZ carbon hygristor sensor for the entire period; Omsk (WMO 28698) used a MARZ goldbeater's skin sensor for the entire period; and King's Park (WMO 45004) used a Vaisala Humicap capacitive sensor from January 1981 on; however, prior to 1981 it used a Vaisala RS18 rolled-hair sensor. Four separate time series, corresponding to each of the four NOAA satellites used during this period, are also plotted in each graph. *NOAA-6* provides coverage from October 1979 through June 1983, *NOAA-7* from Sep-

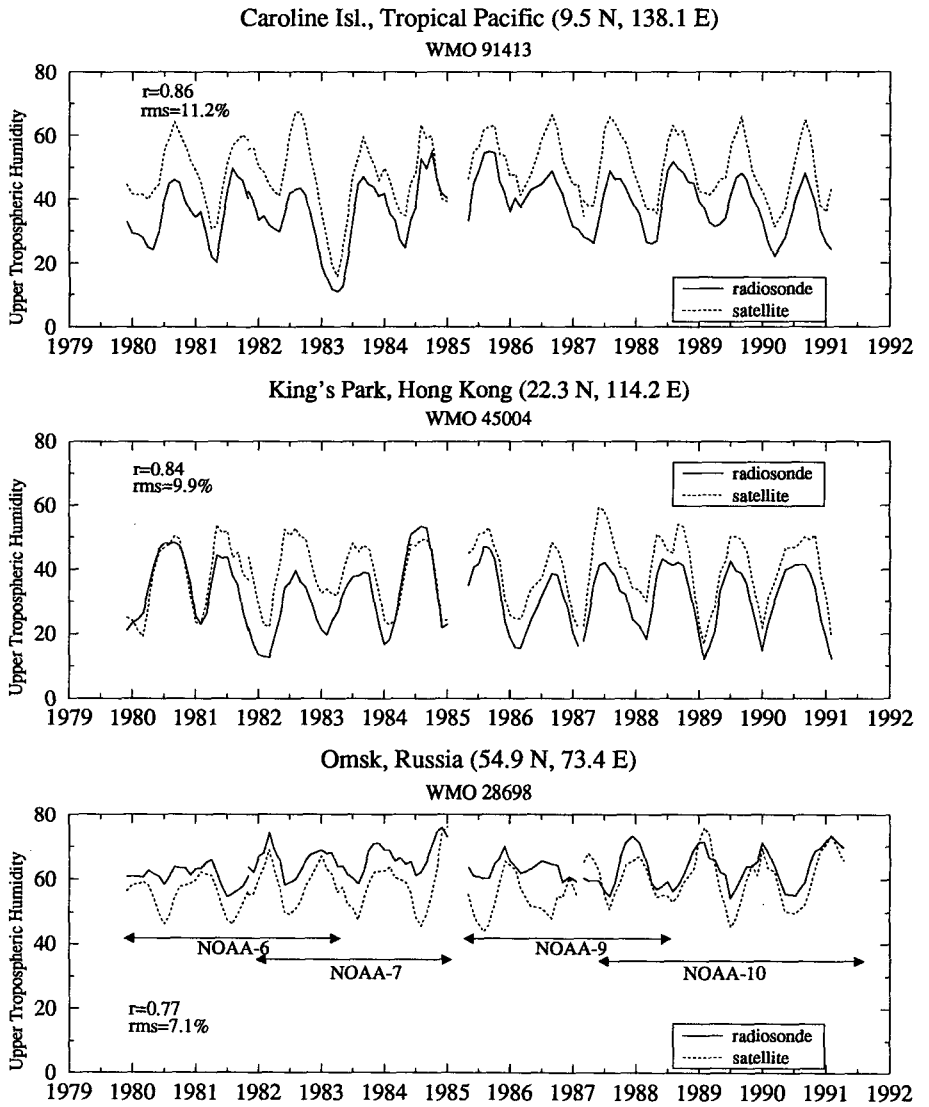

FIG. 10. Time series of satellite (dashed) and radiosonde (solid) UTH in percent for Caroline Islands, tropical Pacific (top), King's Park, Hong Kong (middle), and Omsk, Russia (bottom).

tember 1981 through February 1985, *NOAA-9* from March 1985 through October 1988 (with a gap from March through August 1987), and *NOAA-10* from January 1987 through June 1991. The radiosonde UTH is calculated separately for each satellite using the appropriate spectral response function for that satellite, as described in section 2c. To improve the clarity, each time series was smoothed using a 3-month running average. The mean correlation and rms difference is also shown on each graph. The mean correlation ($\bar{r}$) is an average of the individual correlations (r_i) for each of the four satellite time series (i) weighted by the number of points (n_i) in that time series (see Zar 1974, section 18.5) given by

$$\bar{r} = \tanh\left(\frac{\sum_{i=1}^{4}(n_i - 3)\frac{1}{2}\ln\left(\frac{1 + r_i}{1 - r_i}\right)}{\sum_{i=1}^{4}(n_i - 3)}\right). \quad (3)$$

The mean correlation is determined by transforming the individual correlations to a z-statistic, averaging the z, and then inverse transforming the average z back to a correlation coefficient. This transformation (Fisher's z transformation) is used to transform correlation coefficients to a normally distributed variable (z).

The UTH measurements at all three radiosonde stations exhibit good agreement with the satellite observations. The two tropical stations show very clear sea-

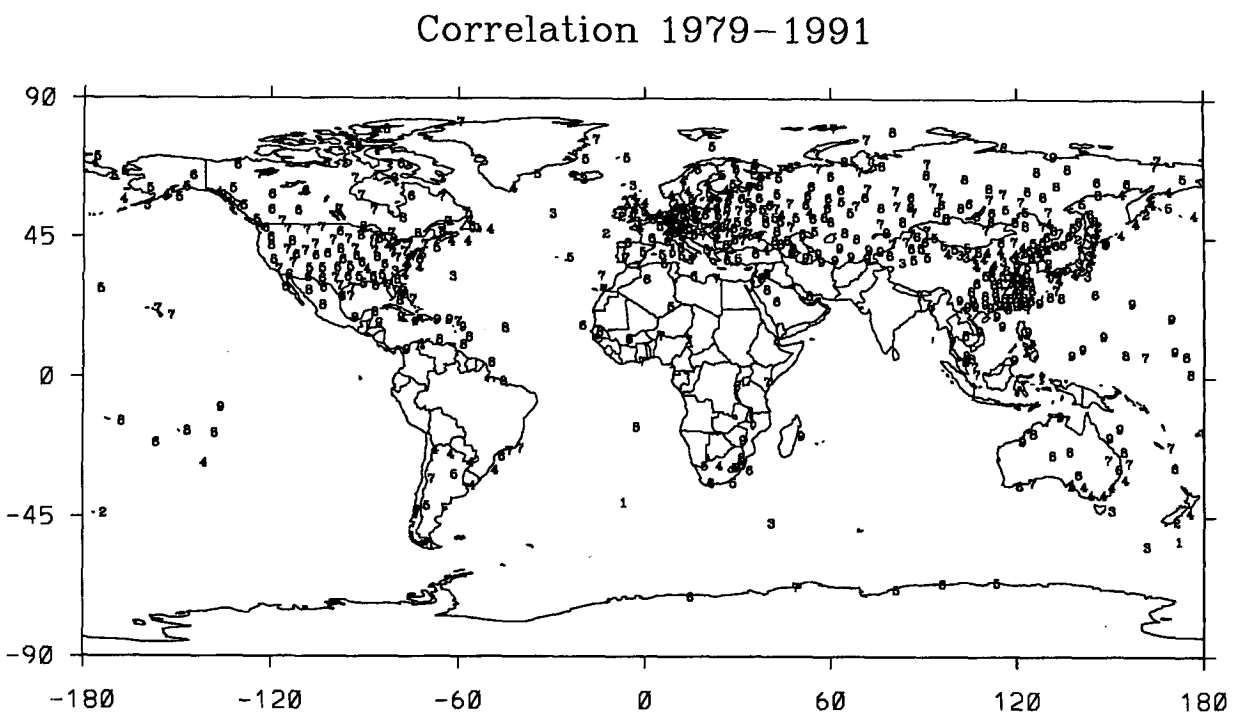

FIG. 11. Map of the weighted-mean temporal correlation ($\bar{r}$) between monthly radiosonde and satellite UTH for the period October 1979–September 1991. Values are multiplied by 10.

sonal variations in both the radiosonde and satellite UTH, while the measurements at the midlatitude station both exhibit distinctly smaller variations. Typical mean correlations ($\bar{r}$) and rms differences are ~0.8 and ~10%, respectively, indicating that all three types of humidity sensors are capable of measuring the temporal variability of upper-tropospheric water vapor reasonably well. The slightly lower correlation and rms difference for Omsk reflect the smaller seasonal variability in UTH for the higher-latitude station and are not necessarily an indication of its performance relative to the other two stations. Note that both the carbon hygristor and capacitive sensors are systematically drier than the satellite measurements, while the goldbeater's skin sensor is systematically moister than the satellite measurements. This is consistent with the results of section 3a. An interesting feature in the Caroline Islands time series is the distinct minimum in both the satellite and radiosonde UTH during February–March 1983. This minimum reflects the drying of the western tropical Pacific during the 1983 El Niño–Southern Oscillation (ENSO) event.

Another intriguing feature is the change in satellite–radiosonde UTH over time in the King's Park time series. Prior to 1981, when the station used a rolled-hair sensor, the radiosonde UTH is in good agreement with the satellite UTH. After 1981, when the station switched to a Humicap sensor, the radiosonde UTH became systematically drier than the satellite UTH. This does not indicate that the rolled-hair sensor was more accurate than the Humicap sensor because the satellite measurements do not serve as an absolute reference (i.e., there may be errors in satellite calibration or in the forward radiance calculations). However, since the satellite measurements do serve as a fixed reference, this comparison does illustrate the discontinuity in the station's record of upper-tropospheric moisture associated with the change in instrumentation. Specifically, the radiosonde UTH becomes drier by about 10% when the sensor was changed from a rolled-hair to a Humicap instrument, which is consistent with the shorter response time of the Humicap sensor. A similar reduction in bias is apparent during 1984, suggesting a return to the rolled-hair sensors although there is no documentation of such a change.

Since only three radiosonde stations are presented, the results shown in Fig. 9 are, of course, not likely to be representative of the entire radiosonde archive. To provide a more complete comparison of the temporal variations in upper-level moisture, Fig. 11 shows a global map of the correlation between monthly mean satellite and radiosonde UTH for the period October 1979–June 1991. The correlation for each radiosonde station is rounded to the nearest tenth and plotted numerically. Roughly 18% of the correlations are greater than 0.8, ~40% range from 0.6 to 0.8, and 35% range from 0.4 to 0.6, with the remaining 7% of the correlations being less than 0.4. Typical rms differences (not

shown) range from 5%–15% and are generally larger over the Tropics where the variability in UTH is greatest. Also note that there is no obvious geopolitical dependence in the correlation map, indicating that the temporal variations are not strongly affected by the regional differences in radiosonde instrumentation. There is a tendency for the correlations to be slightly larger at lower latitudes. This may reflect the fewer and less consequential changes in radiosonde instrumentation over the Tropics as compared to the midlatitudes. Another possibility is that the Tropics could contain a larger signal-to-noise ratio since the amplitude of the annual cycle in UTH, which is the dominant signal in the monthly mean time series, is roughly a factor of 2 to 3 larger over the Tropics than over the midlatitudes (Soden and Bretherton 1995).

4. Spatial sampling bias

In this section we examine the extent to which the limited regional sampling of the radiosonde network affects the upper-tropospheric water vapor climatology. Although the radiosonde network is spatially incomplete, for climatological studies it is often desirable to interpolate the station data onto a global grid using objective analysis techniques (e.g., Oort 1983). Here we use the globally available satellite observations to investigate the impact of the sparse station network upon the reliability of radiosonde-derived global climatological analyses. First the satellite UTH data are sampled at each available radiosonde station for 1989 (e.g., Fig. 3) and then inserted into the objective analysis scheme described by Oort (1983) to interpolate the data onto a 2.5° latitude–longitude grid. The scheme used by Oort is based on an iterative solution of Poisson's equation. It requires that the analyzed gridpoint values satisfy Poisson's equation, subject to the constraints imposed by the observations that serve as internal boundary points. After convergence to a solution, spatial smoothing (filtering) is used to eliminate small-scale noise from the analysis. This sampling procedure provides a picture of what an interpolated satellite UTH field would look like if observations were only made at the radiosonde locations. The station-sampled satellite UTH are then compared with the full-coverage satellite observations to examine the impact of the limited spatial sampling. Although the results shown here employ a particular objective analysis scheme, the differences between various analysis schemes are considered to be small compared to the impact of limited spatial coverage of the radiosonde network.

Figure 12 depicts maps of the full-coverage UTH (top), station-sampled UTH (middle), and the difference (bottom) for July 1989. As expected, the full-coverage and station-sampled maps are in good agreement over North America and Eurasia where the radiosonde coverage is relatively dense. However, in data-sparse

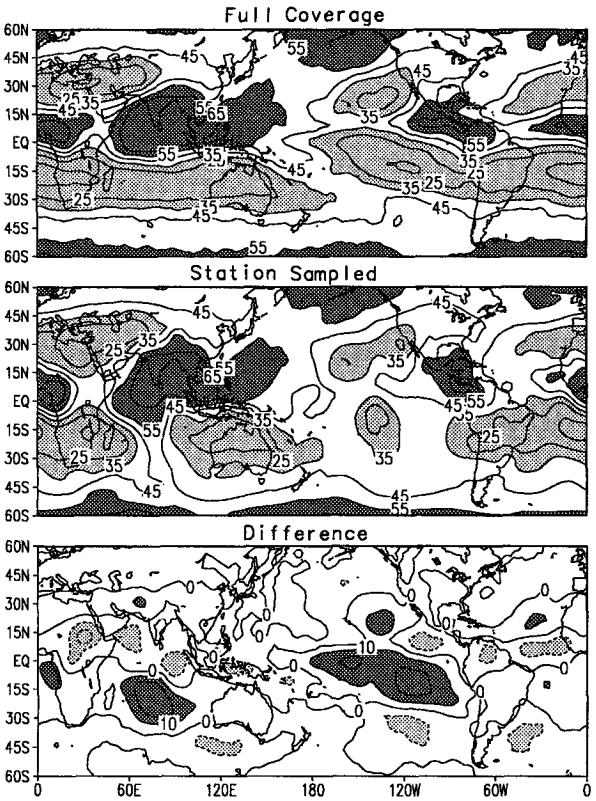

FIG. 12. Map of the satellite UTH for July 1989: full-coverage (top), station-sampled (middle), and the difference (bottom). Contour interval is 10%. For the top and middle map, dark (light) shading indicates values greater (less) than 45% (35%). For the bottom map, dark (light) shading indicates differences greater (less) than 10% (−10%).

regions such as the Tropics, errors in excess of 10% relative humidity result from the limited geographic sampling. For example, along the equatorial ocean belt systematic dry biases of 10%–15% are found over the Atlantic, eastern Pacific, and Indian Oceans, while over the subtropics, particularly in the Southern Hemisphere, systematic moist biases of 10%–20% occur. This suggests that limited spatial sampling tends to reduce the tropical to subtropical moisture gradient. Particularly noteworthy are the large errors (in excess of 20%) noted over the eastern tropical Pacific where there are only a handful of radiosonde stations (see Fig. 3). Adequate coverage in this area is especially critical for determining moisture variations associated with ENSO. This is demonstrated in Fig. 13, which compares the change in UTH during the 1983 ENSO warm event as determined from the full-coverage and station-sampled satellite data. The top panel depicts the DJF 1983 minus DJF 1985 UTH from the full-coverage observations, and the bottom panel shows the UTH difference from station-sampled data. The chief feature in the full-coverage observations is the distinct moist anomaly of 10%–20% over the eastern equatorial Pa-

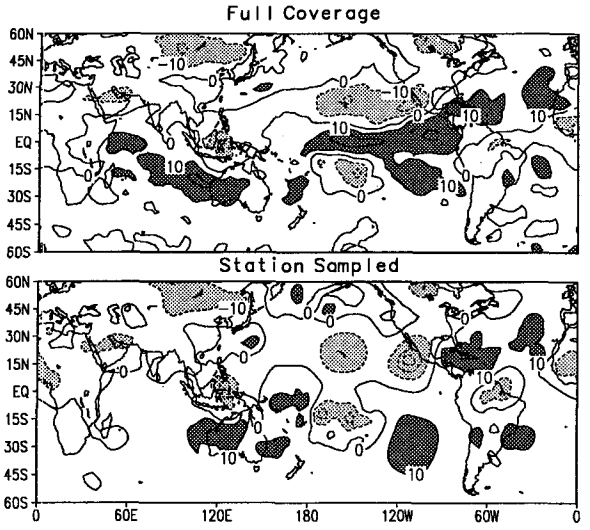

FIG. 13. Change in upper-tropospheric humidity associated with the 1983 ENSO. Maps display the UTH difference (DJF 1983 − DJF 1985) for full coverage (top) and station sampled (bottom). Contour intervals are 10%. Dark (light) shading indicates differences greater (less) than 10% (−10%).

cific associated with the eastward shift of deep convection during the 1983 ENSO event. However, this feature is completely absent in the station-sampled UTH field (as is the anomaly in the equatorial Indian Ocean), demonstrating that sampling limitations can introduce large regional biases in the tropical radiosonde climatology. Furthermore, this comparison suggests that the radiosonde network presently lacks sufficient coverage, particularly in the eastern tropical Pacific, to accurately capture ENSO-related variations of upper-tropospheric water vapor.

5. Clear-sky sampling bias

Due to the strong attenuation of IR radiation by clouds, satellite estimates of the upper-tropospheric humidity are not available in conditions of extensive cloud cover. The radiances examined here are derived using the N^* cloud-clearance technique, which analyzes pixel radiances (~20-km nadir resolution) to provide estimates of the clear-sky radiance averaged over a region of roughly 200 × 100 km in conditions of up to 75% cloud cover. However, since clouds are likely to be correlated with relative humidity, the restriction of information to clear and partially overcast conditions is likely to introduce a systematic dry bias into the satellite climatology. In this section, we attempt to quantify this bias by comparing the total-sky radiosonde climatology of UTH with a corresponding clear-sky radiosonde climatology containing the identical sampling restrictions present in the satellite data.

Figure 14 shows a histogram of the difference between the total-sky UTH (i.e., the UTH averaged over both clear and cloudy conditions) and the corresponding clear-sky UTH. Both the total- and clear-sky UTH are determined from a 3-month average of the daily radiosonde data for the period June, July, and August 1989. The clear-sky UTH was determined by replicating the same sampling bias present in the satellite data. That is, the clear-sky average is composed of only those radiosonde UTH for which there was a corresponding clear-sky satellite radiance available for that day and location. In doing the averaging, we required that at least one of the two satellite orbital passes contain a clear-sky observations for a given day. If this criterion was met, then the average of the radiosonde 0000 and 1200 UTC UTH was used to define the radiosonde clear-sky UTH for that day. No attempt was made to determine the radiosonde launch closest to the corresponding satellite overpass.

As expected, the clear-sky UTH tends to be systematically smaller than the total-sky UTH, suggesting that the lack of measurements from overcast environments introduces a systematic dry bias into the satellite climatology. The magnitude of this bias is fairly small, typically about 4% and usually less than 10% in terms of the relative humidity. The relatively small bias may reflect the fact that the UTH corresponds to an average relative humidity over a layer several kilometers thick (see Fig. 1), whereas the majority of upper-level clouds (e.g., cirrus and cirrostratus) are considerably thinner than this. Thus, it is unlikely that the entire layer to which the UTH is sensitive will be saturated when a cloud is present. It is also important to emphasize that these results correspond to the total-sky minus clear-sky bias, where the total sky is the sum of cloudy- and clear-sky observations. The cloudy-sky minus clear-sky differences would be considerably larger. Finally, we note that these estimates of clear-sky bias are reasonably consistent with those obtained by Gaffen and Elliott (1993), who compared clear and total-sky ra-

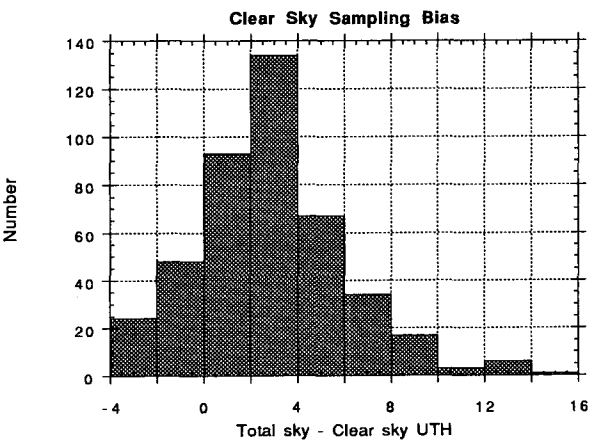

FIG. 14. Histogram of total-sky minus clear-sky UTH in percent determined from radiosonde data for JJA 1989.

diosonde climatologies of column-integrated water. Their results suggest that the lack of observations from overcast skies introduces a fractional dry bias in precipitable water of roughly 0.05 to 0.15. That is, if we consider a profile with a vertically uniform relative humidity of 50%, the results of Gaffen and Elliott would suggest a clear-sky bias in relative humidity of 2.5%–7.5% for that profile. We find a bias in UTH of ~4%. This is not intended to suggest that a profile of constant relative humidity equal to 50% is typical, rather this example is simply meant to place results of Gaffen and Elliot into the context of the present study.

It is also worth noting that a small fraction (approximately one-sixth) of the differences are negative. The cause of this is not clear. One possible explanation is that the clear-sky radiances used here are not available in conditions of extensive cloud cover, even if that cloud cover is restricted to the lower atmosphere. If the water vapor at upper levels is negatively correlated with low cloud cover, this could yield a negative sampling bias in areas with extensive low-level cloud. For example, this could occur in the cold sector of extratropical cyclones where low clouds are associated with upper-level subsidence (e.g., see Fig. 7 of Lau and Crane 1995). Alternatively, it is also possible that the water vapor at upper levels is uncorrelated with low cloud cover (i.e., the true clear-sky sampling bias is zero) and that the negative correlations simply reflect "noise" due to, for example, differences between the times of the satellite overpass and the times of the radiosonde launches.

Finally, due to the uneven distribution of radiosonde locations, the estimates of the clear-sky bias are heavily weighted toward the Northern Hemisphere midlatitudes. Inspection of the geographic distribution of the estimated biases indicates no obvious regional dependence (not shown). Nevertheless, these estimates should be regarded as tentative results that may need revision as new information on the total-sky water vapor distribution becomes available from instruments such as the microwave limb sounder.

6. Discussion

An improved understanding of the role of upper-tropospheric water vapor in the climate system requires an accurate assessment of our ability to monitor humidity on a global scale. Toward this end, we compared the climatological variations of upper-tropospheric relative humidity determined from the global radiosonde network and from satellite infrared measurements. These datasets represent two of the most extensive moisture climatologies available and have very complementary sampling characteristics, enabling an investigation of the strengths and weaknesses of each.

Comparison of the regional distribution of upper-tropospheric humidity reveals a pattern of discrepancy that exhibits a strong geopolitical dependence. Radiosondes over the former Soviet Union, China, and eastern Europe indicate a systematically moister upper-troposphere relative to the satellite observations, whereas radiosondes over most other locations indicate a systematically drier upper troposphere. This pattern of discrepancy is largely a result of differences in radiosonde instrumentation. This study indicates that radiosondes equipped with goldbeater's skin sensors report relative humidities that are roughly 18%–20% higher than radiosondes equipped with capacitive or carbon hygristor sensors. This feature is attributable to the greater response time for the goldbeater's skin sensor relative to the other sensors. This bias is found to be greater in the upper troposphere than in the midtroposphere, consistent with a decrease in response time with decreasing height. The bias is also observed to be greater during JJA (~18%) than DJF (~15%). When the different radiosonde types are considered individually, the regional variations in upper-tropospheric humidity between satellite and radiosonde climatologies are in good agreement ($r \sim 0.8$).

Temporal variations of upper-tropospheric humidity measured by the radiosonde and satellite instruments are also well correlated and exhibit much less dependence upon radiosonde instrumentation. Both the pattern of seasonal change and the monthly mean time series of upper-tropospheric water vapor are shown to be in reasonably good agreement (see section 3b). Assessing the accuracy of trends in upper-tropospheric water vapor over the last decade and a half requires a more detailed and careful analysis of each dataset. Such an investigation is presently in progress at GFDL.

The impact of limited spatial coverage upon the radiosonde climatology was also investigated. Over the northern midlatitudes, where the radiosonde coverage is greatest, spatial sampling limitations have little impact upon the moisture climatology. However, over data-sparse regions such as the Tropics, the limited spatial coverage can introduce systematic errors of 10%–20% in terms of the relative humidity. This problem is particularly severe in the eastern tropical Pacific, which is largely void of any radiosonde stations yet is especially critical for monitoring interannual variability (e.g., ENSO). This study suggests that the radiosonde network presently lacks sufficient coverage in the eastern tropical Pacific to accurately capture ENSO-related variations of upper-tropospheric water vapor. The restricted spatial sampling may perhaps represent the most significant limitation to the radiosonde climatology because, unlike instrumentation problems, there is no obvious way to correct for these shortcomings.

One limitation to the satellite water vapor measurements is the restriction of observations to clear and partially cloudy conditions. While this limitation is widely recognized, there has been little effort to quantify the impact that it has upon the satellite moisture climatology. We investigated the magnitude of this bias by imposing the same clear-sky sampling restrictions present

in the satellite measurements upon the radiosonde data and then comparing the clear-sky and total-sky radiosonde UTH. This comparison suggest that the lack of observations in areas of extensive cloud cover introduces a modest dry bias in the satellite climatology that is typically about 4% and usually less than 10% in terms of relative humidity. These results are consistent with those of Gaffen and Elliott (1993), who examined differences between clear-sky and total-sky precipitable water.

Acknowledgments. We thank Abraham Oort for his encouragement and many valuable discussions during the course of this study. We also acknowledge helpful advice and suggestions from Bill Blackmore, Francis Bretherton, Bill Elliott, Dian Gaffen, Isaac Held, Tom Karl, Jerry Mahlman, Jose Piexoto, Gary Wade, and two anonymous reviewers.

REFERENCES

Bates, J. J., and X. Wu, 1996: Interannual variability of upper-troposphere water vapor band brightness temperature. *J. Climate,* **9,** 427–438.

Elliott, W. P., and D. J. Gaffen, 1991: On the utility of radiosonde humidity archives for climate studies. *Bull. Amer. Meteor. Soc.,* **72,** 1507–1520.

Eyre, J. E., 1991: A fast radiative transfer model for satellite sounding systems. ECMWF Tech. Memo. 176, 28 pp.

Gaffen, D. J., 1993: Historical changes in radiosonde instruments and practices. World Meteorological Organization/TD-No. 541, Rep. No. 50, 123 pp.

——, and W. P. Elliott, 1993: Column water vapor content in clear and cloudy skies. *J. Climate,* **6,** 2278–2287.

Garand, L., C. Grassotti, J. Halle, and G. L. Klein, 1992: On differences in radiosonde humidity-reporting practices and their implications for numerical weather prediction and remote sensing. *Bull. Amer. Meteor. Soc.,* **73,** 1417–1423.

Goody, R. M., 1964: *Atmospheric Radiation.* Vol. I, *Theoretical Basis.* Oxford University Press, 436 pp.

Kidwell, K. B., 1991: NOAA polar orbiter data users guide. NOAA/NESDIS, 245 pp.

Lau. N.-C., and M. W. Crane, 1995: A satellite view of the synoptic-scale organization of cloud cover in midlatitude and tropical circulation systems. *Mon. Wea. Rev.,* **123,** 1984–2006.

McCormick, M. P., and E. W. Chiou, 1994: Climatology of water vapor in the upper troposphere and lower stratosphere determined from SAGE II observations. Preprints, *5th Symp. on Global Change Studies,* Amer. Meteor. Soc., Nashville, 213–215.

McMillin, L. M., and C. Dean, 1982: Evaluation of a new operational technique for producing clear radiances. *J. Appl. Meteor.,* **21,** 1005–1014.

Middleton, W. E. K., and A. F. Spilhaus, 1953: *Meteorological Instruments.* University of Toronto Press, 286 pp.

Monine, P., A. Chedin, and N. A. Scott, 1987: Automatic classification of air mass type from satellite vertical sounding data: Application to NOAA-7 observations. *Ocean–Air Interactions,* **1,** 95–108.

Murty, D. G. K., W. L. Smith, H. M. Woolf, and C. M. Hayden, 1993: Comparison of radiances observed from satellite and aircraft with calculations using two atmospheric transmittance models. *J. Appl. Opt.,* **32,** 1620–1628.

Nash, J., and F. Schmidlin, 1987: WMO international radiosonde comparison, instruments and observing methods. WMO/TD-No. 195, Rep. No. 30, 103 pp.

Oakley, T., 1993: Instruments and observing methods. World Meteorological Organization/TD-No. 587, Rep. No. 56, 90 pp.

Oort, A. H., 1983: *Global Atmospheric Circulation Statistics, 1958–1973.* NOAA Prof. Paper No. 14, NOAA, U.S. Dept. of Commerce, Rockville, MD, 180 pp.

Salathe, E. P., D. Chesters, and Y. C. Sud, 1995: Evaluation of the upper-tropospheric moisture climatology in a GCM using TOVS radiance observations. *J. Climate,* **8,** 2404–2414.

Schmetz, J., and O. M. Turpeinen, 1988: Estimation of the upper tropospheric relative humidity field from METEOSAT water vapor image data. *J. Appl. Meteor.,* **27,** 889–899.

Soden, B. J., and F. P. Bretherton, 1993: Upper tropospheric relative humidity from the GOES 6.7 μm channel: Method and climatology for July 1987. *J. Geophys. Res.,* **98,** 16 669–16 688.

——, and ——, 1994: Evaluation of the water vapor distribution simulated in GCMs using satellite observations. *J. Geophys. Res.,* **99,** 1187–1210.

——, and R. Fu, 1995: A satellite analysis of deep convection, upper-tropospheric humidity, and the greenhouse effect. *J. Climate,* **8,** 2333–2351.

——, and F. B. Bretherton, 1996: Interpretation of TOVS water vapor radiances in terms of layer-average relative humidities: Method and climatology for the upper, middle, and lower troposphere. *J. Geophys. Res.,* in press.

——, S. A. Ackerman, D. O'C. Starr, S. H. Melfi, and R. A. Ferrare, 1994: Comparison of upper tropospheric water vapor from GOES, Raman lidar, and CLASS measurements. *J. Geophys. Res.,* **99,** 21 005–21 016.

Wade, C. G., 1995: Calibration and data reduction problems affecting National Weather Service radiosonde humidity measurements. Preprints, *Ninth Symp. on Meteorological Observations and Instrumentation,* Charlotte, NC, Amer. Meteor. Soc., 37–42.

Weinreb, M. P., H. E. Fleming, L. M. McMillan, and A. C. Neuendorffer, 1981: Transmittance for the TIROS operational vertical sounder. NOAA Tech. Rep. 85, 66 pp.

Wu, X., J. J. Bates, and S. J. S. Khalsa, 1993: A climatology of the water vapor band brightness temperature from NOAA operational satellites. *J. Climate,* **6,** 1282–1300.

Zar, J., 1974: *Biostatistical Analysis.* Prentice-Hall, 620 pp.